Polymer Degradation and Stability 151 (2018) 1–11

Contents lists available at ScienceDirect

Polymer Degradation and Stability

journal homepage: www.elsevier.com/locate/polydegstab

Hydrolytic degradation kinetics of bisphenol E cyanate ester resin and composite

James A. Throckmorton[a], Greg Feldman[a], Giuseppe R. Palmese[a], Andrew J. Guenthner[b,*], Kevin R. Lamison[c], Neil D. Redeker[c], Patrick N. Ruth[c]

[a] Drexel University Department of Chemical and Biological Engineering, 3141 Chestnut Street, Philadelphia, PA, United States
[b] Air Force Research Laboratory, 10 E. Saturn Blvd, Edwards AFB, CA, United States
[c] ERC Incorporated, 10 E. Saturn Blvd, Edwards AFB, CA, United States

ARTICLE INFO

Keywords:
Hydrolysis
Polycyanurates
Cyanate ester
Near-IR
Thermosets
Kinetics

ABSTRACT

Cyanate ester resin systems offer promise for many high-temperature polymer applications, but the potential for many applications is limited due to hydrolytic degradation of the cured polymer network, which can blister the resin, decrease its cross-linking density, and reduce the maximum allowable use temperature. This study examines the hydrolytic degradation of a Bisphenol E dicyanate ester (LECY) and a glass-fiber composite of LECY. Equilibrium water sorption, reaction rates, and glass transition temperature changes are monitored. Despite differences in diffusion and sorption, the glass fiber composite is shown to behave similarly to the neat polymer system in terms of degradation. Results were compared to PT-30 triphenolic cyanate ester, and LECY was determined to have lower equilibrium water sorption values, and a lower degradation rate.

1. Introduction

Bisphenol-based cyanate esters [1,2] are rigid thermosetting resins that generally exhibit high glass transition temperature (Tg), good fracture toughness, excellent substrate adhesion, low shrinkage, low dielectric loss, and low moisture uptake [3]. These properties make them attractive replacements for common thermosetting systems such as epoxies or maleimides for applications in the aerospace, communications, and microelectronics industries. In some applications, such as lightweight structures aboard spacecraft [4–6], concerns about moisture uptake in cyanate esters are mainly limited to concerns about outgassing. In others, such as radomes [7,8], the effect of moisture uptake and network hydrolysis on properties such as dielectric loss is a significant concern. In addition to impacts on dielectric performance [9], in microelectronic applications [10,11], hydrolysis also impacts adhesion properties on metal substrates and reduces the glass transition temperature (T_g), which must remain above hot solder temperatures for proper performance. Hydrolysis products can also lead to blistering and component failure [12]. Many of these same concerns can be found in other applications such as photonics [13,14] and radiation-resistant magnets for particle accelerators [15,16] and thermonuclear fusion reactors [17–25].

Both monomers (containing the cyanate ester functional group) and the cured resin (containing triazine rings) are conventionally referred to as cyanate ester resins. They are formed in excellent yields by the reaction of corresponding phenols with cyanogen halide [26]. Upon heat treatment, a polycyclotrimerization reaction occurs that can be accelerated by the use of a metallic and hydroxyl catalysts to form a highly crosslinked network with the cyanurate ring at the crosslink junction [3,26–29].

Early tests showed that multilayer cyanate ester laminate parts failed when stored under high humidity conditions [27]. Although cyanate esters absorb less moisture than epoxies, the blister time for moisture-conditioned cyanate ester boards can be less than that of epoxy boards [12]. Additional studies established a significant reduction in glass transition temperature upon humidity conditioning, limiting the potential of cyanate esters for high temperature applications. Kasehagen et al. demonstrated that both phenomena are related to a chain scission hydrolysis reaction that degrades the network structure when wet material is exposed to high temperature conditions [12]. They proposed a mechanism for the hydrolysis reaction and derived the reaction kinetics from calorimetry. They found that the primary degradation mechanism of cyanate ester resins proceeded via hydrolysis of the aryl ether bonds, followed by decomposition, yielding phenols, carbon dioxide and ammonia as the final hydrolysis products. A schematic representation for the degradation reaction was proposed by Kasehagen et al. and is shown in Fig. 1 [12].

Lin et al. report the same phenomenological observations - water

* Corresponding author.
E-mail address: andrew.guenthner@us.af.mil (A.J. Guenthner).

https://doi.org/10.1016/j.polymdegradstab.2018.02.009
Received 16 November 2017; Received in revised form 27 January 2018; Accepted 12 February 2018
Available online 16 February 2018
0141-3910/ Published by Elsevier Ltd.

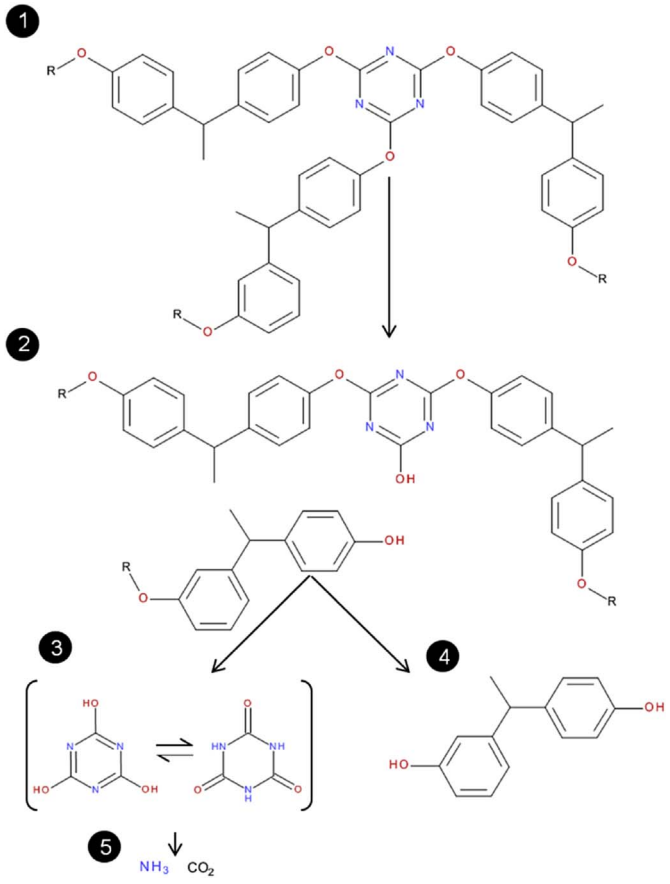

Fig. 1. Full hydrolytic degradation of LECY cured network, featuring the fully formed network (1), after a single hydrolysis event, a triazine alcohol and phenol are created and a single cross-link is removed (2), the tautomeric forms of cyanuric acid (3), the bisphenol degradation product (4), and the final degradation products – ammonia and carbon dioxide (5).

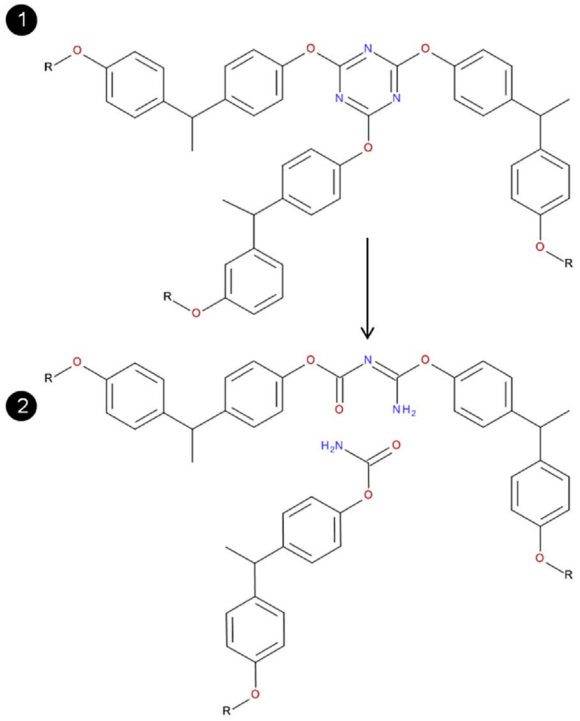

Fig. 2. Alternative degradation scheme following Lin et al. [30] Under this scheme, 2 mol of water hydrolyze the triazine ring, producing a primary carbamate and a dimer linkage.

uptake, hydrolysis, and T_g reduction for cyanate esters conditioned at 60 °C/100% RH [30]. In contrast to Kasehagen, they proposed that water decomposes the triazine ring rather than breaking an aryl ether bond, through a reverse-polymerization reaction that produces an aminated isocyanate. This mechanism is shown in Fig. 2. It should be noted that these network-degradation reactions are distinct from the hydrolytic carbamate formation of uncured cyanate ester groups commonly studied as a cyanate ester degradation pathway [31–33].

This study follows the methods of Marella et al. [34] and aims to understand the mechanism and reaction kinetics of highly cured cyanate ester degradation by studying cyanate ester resins in hot/wet conditions using a combination of reversible and irreversible gravimetric sorption, Fourier-transform infrared spectroscopy (FTIR), and T_g change by dynamic mechanical analysis (DMA). Other studies have identified the final degradation products, as phenol, carbon dioxide and ammonia [35,36]; this investigation concentrates mainly on the formation of intermediate products – phenols, cyanuric acid and bisphenol, by mass uptake and FTIR, as well as on methods to quantitatively link changes in mass, hydrolysis rates, and the decrease in T_g associated with hydrolysis.

2. Materials and methods

2.1. Materials

The dicyanate ester of bisphenol E, which has the chemical name 1,1-bis(4-cyanatophenyl)ethane, and the trade name Primaset® LECY, was supplied by Novoset and stored at 4 °C in a low humidity environment. The as-received bisphenol E dicyanate ester was catalyzed with 2.0 phr of a 30:1 (by weight) mixture of nonlyphenol (Aldrich, 97%) and copper (II) acetylacetonate (Research Organic/Inorganic Chemicals Inc.), with a total copper concentration of 160 ppm by weight. Catalyst batches were formulated by first dissolving the copper (II) acetylacetonate in the nonylphenol at 60 °C by stirring for 1 h, and then storing under ambient conditions for up to 30 days. The chemical structures for nonylphenol, bisphenol E dicyanate ester, and copper (II) acetylacetonate are shown in Fig. 3.

2.2. Methods

2.2.1. Neat resin casting and cure

Just prior to cure, the resin and catalyst were mixed at room temperature and de-gassed under vacuum for 30 min. The de-gassed mixture was then poured into a 75 × 87 mm vertical mold cavity formed by inserting a 1.5 mm thick U-shaped aluminum spacer between two sheets of Teflon-coated aluminum. The pieces were clamped together and held with the long axes of the cavity in the vertical position for the

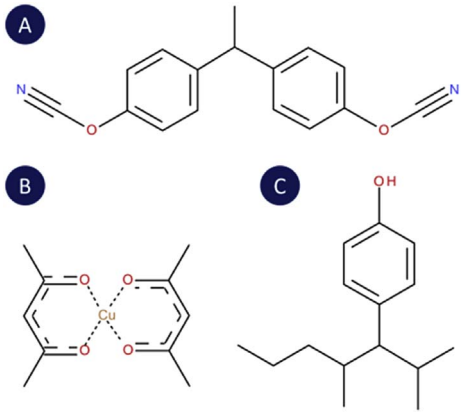

Fig. 3. Bisphenol E dicyanate ester (A), Copper (II) acetylacetonate (B), and nonylphenol (C).

cure. After carefully pouring in the catalyzed resin, the mold was placed into an oven under flowing nitrogen and held at 150 °C for 1 h and 190 °C for 3 h. At the end of the cure cycle, the clamps holding together the mold were loosened and the mold was allowed to cool slowly to near room temperature, at which point the part was de-molded. The cured slab was then post-cured free-standing at 240 °C for 1 h under nitrogen.

2.2.2. Fiber-reinforced composite hand lay up and cure

Glass-fiber reinforced composite panels measuring 4″ x 4″ were fabricated and cut into specimens using the following procedure. To prepare a single panel, Hexcel S3325 woven glass fabric (nomenclature 4522-30-F81) was cut into 16 oversized pieces using the plunger of a 1 ton Tetrahedron compression molding machine as a template and adhesive tape to secure the areas immediately adjacent to cuts. The oversized pieces were stacked into two balanced assemblies with eight plies each using a fiber orientation pattern of 0°,90°,45°,-45°,-45°,45°,90°,0°, where 0° refers to the warp direction and positive numbers indicate a clockwise rotation when the interior surface of the fabric roll faces the observer. One assembly was designated for use as the panel reinforcement, while the other was designated for use as a bleeder.

The mold utilized was a two-piece 4″ x 4” “picture frame” type with a bottom plate. Three pieces of 0.005″ Teflon film were cut, two slightly oversized for the panel dimensions, and one to match the panel (e.g. mold interior) dimensions. The Teflon film matching the panel dimensions was then perforated with 1/16″ holes in a rectangular grid with spacing of about ½”. To create the molding assembly, a non-perforated Teflon film was placed at the center of the surface of the lower mold plate, which was placed on the lower platen of the press. The eight-layer bleeder stack was then laid onto the film and cut to size using the picture frame portion of the mold and a scalpel, until the bleeder assembly fit within the mold. The bleeder assembly was then weighed and set aside, and the picture frame portion of the mold removed. A small pool of catalyzed LECY (at ambient temperature) was then poured onto the Teflon film remaining on the mold bottom plate. The first layer of reinforcement was then gently placed on top, and resin was worked into the fabric using a rubber squeezing rod. The process was repeated for each layer, with additional resin added when dry spots appeared or reinforcement without resin added when pools of excess resin appeared. After all eight layers were in place, the other non-perforated Teflon film was placed on top, and additional squeezing was used to consolidate the laminate.

Using the plunger as a rough template and the picture frame portion of the mold for final adjustments, excess material was removed from the outer portions of the laminate with the aid of a scalpel, until the laminate fit within the picture frame mold. The picture frame was then placed around the laminate and mechanically fastened on to the bottom plate. The upper non-perforated Teflon film was then set aside and replaced with the perforated Teflon film. The bleeder layers were then added, and the non-perforated Teflon film was then placed at the top of the stack. The plunger was then put in place, and additional Teflon film was applied liberally to the surrounding metal surfaces. The press was then closed.

The cure cycle for the compression molded laminate was as follows: ramp at 5.5 °C/min. to 90 °C, hold at 90 °C for 90 min, ramp at 5.5 °C/min. to 250 °C, hold at 250 °C for 240 min, then ramp at 5.5 °C/min to 27 °C. To extract the part, the mold and plunger were removed from the press. The bottom plate was then unfastened from the picture frame and removed with ease. The remaining plunger, frame, and laminate were then placed into a hand-operated hydraulic press, and the plunger was utilized to eject the laminate from the frame with minimal force. The panel was then separated from the bleeder.

2.2.3. Sample preparation and dimensions

Post-cured slabs of both neat resin and fiber-reinforced composite were cut into identical sections using a Struers precision saw with a diamond cut-off wheel rotating at 4000 rpm and a linear rate of travel of 0.3 mm/s. Neat resin samples were made in two sizes. Sample type “LECY 1” (25 × 9.5 × 1.5 mm) and “LECY 2” (38.6 × 10.4 × 3 mm) were rectangular bars with differing thickness (used to probe the dynamics of water diffusion). In addition, samples of the LECY/Fiberglass hand layup were also cut into rectangular bars (34.7 × 10 × 2.1 mm). After cutting, all samples were dried at 110 °C for 48 h.

2.2.4. Water uptake studies

Water uptake studies were conducted on each of the 1.5 mm thick samples. At least six samples of each polymer resin block were prepared, and dried at 110 °C for 48 h. The dried samples were treated environmentally in either boiling water or an Associated Environmental Systems LH-1.5 Humidity chamber at 85 °C (± 0.5 °C) with a relative humidity of 85% (± 2%).

For the first sample set, a 3 neck round bottom flask with a condenser and a thermometer was half filled distilled water and heated to boiling, and the samples were immersed in the boiling water. For all other samples, the samples were placed in an environmental humidity chamber set at a constant 85 °C/85% RH. Samples were taken out at regular time intervals (“wet” samples), wiped to remove surface water, and weighed. After weighing, a near FTIR spectrum of each sample was recorded using a Nicolet Nexus 670 near-FTIR spectrometer.

At intervals of one week, one sample was removed from the boiling water and placed in a 100 °C oven for 48 + hours until dried (“dry” samples). FTIR spectra were recorded to differentiate the diffusion of water and the formation of hydroxyl bonds due to hydrolysis. A dynamic mechanical analyzer (DMA) was used to monitor the changes in T_g resulting from the degradation reaction.

Mass was determined by an Ohaus Explorer Pro 214CN lab balance (accurate to 0.0001 g). The fractional mass gain m_r after each measurement was calculated by:

$$m_r = (m - m_0)/m_p$$

where m, m_0, and m_p denote the sample mass after exposure, mass at start of exposure, and mass of polymer in the sample, respectively.

2.2.5. Fourier transform-near infrared spectroscopy

Absorbance spectra were obtained using a Nicolet Nexus 670 near FTIR spectrometer. Near infrared (NIR) spectroscopy was chosen for analysis instead of mid-infrared due to the separation between the –OH (5000 cm^{-1} and 6950 cm^{-1}) and H_2O (5250 cm^{-1}) peak locations, and the ease of sample preparation and averaging enabled by the lower absorbance of NIR radiation in these samples. The instrument uses a Germanium/KBr beam splitter and a deuterated tryglycine sulfate (DTGS) detector at 8 cm^{-1} resolution, 32 scans/sample and a spectral range of 8000–4000 cm^{-1}. The spectrometer was used in transmission mode, with the FTIR beam passing directly through the sample. Quantitative analyses of the concentrations of species of interest were conducted using heights of the peaks of interest normalized to the height of an aromatic reference peak near 6000 cm^{-1}. In order to accomplish this in a reproducible way, for each individual set of data being analyzed, a representative wavenumber for a given peak appearing in that particular set of data was chosen (for instance, 5236 cm^{-1} for the –OH peak and 5998 cm^{-1} for the aromatic reference peak). The absorbance values corresponding to these wavenumber locations on each spectrum in the set were used for each analysis. These values are provided in the figure captions that correspond to each analysis performed. The values chosen varied slightly for different analyses, reflecting slight differences in the characteristic peak location, for instance, between wet and dry samples.

2.2.6. Dynamic mechanical analysis

The glass transition temperature of samples was determined using a Dynamic Mechanical Analyzer (TA Instruments model DMA Q800) in

single cantilever bending mode. Typical temperature ramping tests were conducted from 30 to 340 °C, with a heating rate of 2 °C per min, an oscillation frequency of 1.0 Hz, and amplitude of 13 μm.

3. Results

Three experimental techniques – mass uptake, near-FTIR, and dynamic mechanical analysis, are used to determine the kinetics, nature, and extent of network degradation by hydrolysis. Mass uptake, measured throughout a wet and dry sample conditioning schedule, provides a quantitative assessment of the interaction between water and the polymer network. This mass uptake can be understood as additive contributions from environmental water sorption and hydrolysis product formation. Near-FTIR identifies the presence of hydrolysis products and bulk water, allowing for analytical determination of the two mass uptake effects. Additionally, for the experimental setup utilized, near- FTIR provides a more precise measure of hydrolysis product formation than mass uptake. Finally T_g measurements by dynamic mechanical analysis allow for a correlation between network degradation and functional property loss.

3.1. Mass uptake

Fig. 4 shows the relative weight change of the samples under an environmental conditioning regimen of moisture exposure and drying conditions. Samples were placed in a moisture environment for up to six weeks, with one sample removed for drying each week (represented by the curves descending from the total mass uptake curve). Results for LECY conditioned in continuously boiling water are presented in Fig. 4a. 1.5 mm- and 3 mm-thick LECY samples exposed to a constant 85 °C/85% RH environment in a humidity chamber are shown in Fig. 4b and c, respectively. Fig. 4d shows the results of a LECY/glass fiber composite (30% LECY by mass) exposed to a 85 °C/85% RH humidity environment.

For all polymer samples, relative mass uptake was determined by:

$$m_r = \frac{m - m_0}{m_p} \quad (1)$$

where m_r is relative mass uptake, m is measured mass of the conditioned sample, m_0 is the total mass of the original sample, and m_p is the mass of polymer in the original sample. For non-composite polymer samples, $m_0 = m_p$. For the glass fiber composite sample, $m_p = m_0 x 0.30$ to represent the polymer fraction of the composite.

All samples exhibit similar general behavior. Initially, there is an uptake of ~2% within the first 48 h. This varies slightly sample to sample, with a higher uptake for the boiling water and the glass fiber samples than for the 85 °C/85% RH LECY samples. After that initial uptake, mass continues to increase linearly, gaining another 0.5% points in mass over the next six weeks. Most of the mass uptakes were reversible when samples were exposed to a dry environment. This reversible portion was taken to be absorbed water. Additionally, all samples showed some irreversible mass increase that remained in the sample after drying. This was taken to be additional mass from hydrolysis product formation, as shown in Fig. 1.

3.2. FTIR

FTIR spectroscopy reveals additional information about

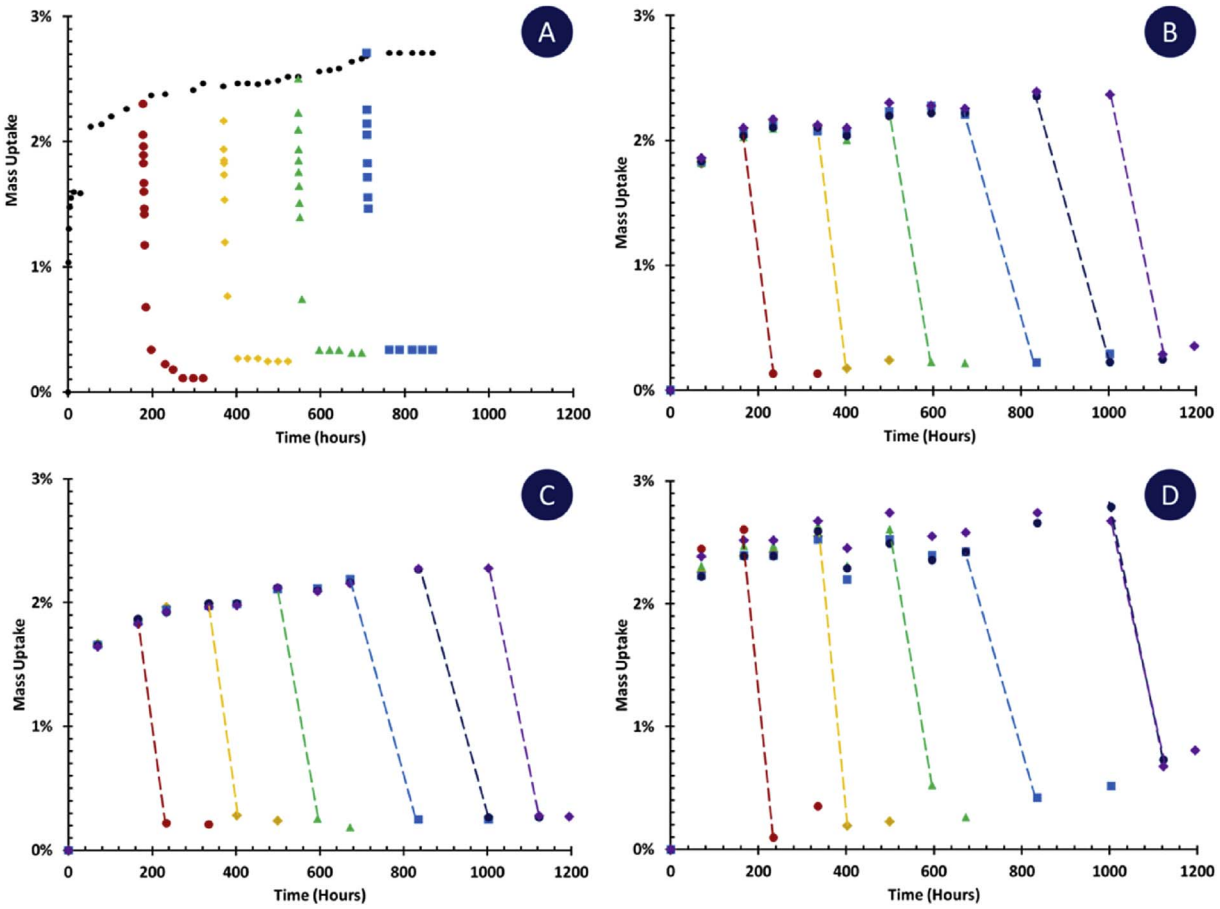

Fig. 4. Relative mass uptake and drying curves for LECY 1 in boiling water (A), LECY 1 in 85/85% RH (B), LECY 2 in 85/85% RH (C), and LECY/GF in 85/85% RH (D). For each curve, the top line shows the mass uptake of the samples in the humidity environments. The descending curves are the masses of samples that are removed from a humidity environment and placed in a dry oven at 110 °C.

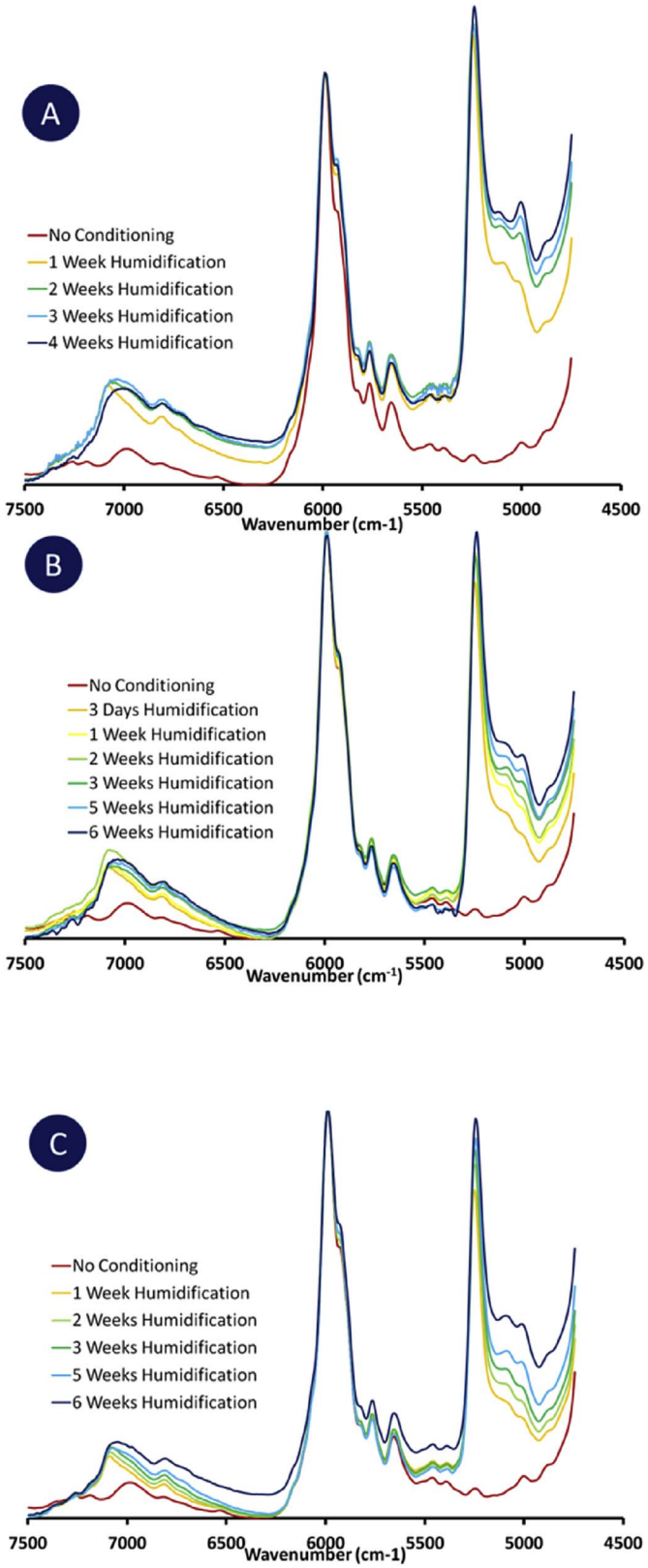

Fig. 5. FTIR spectra for wet samples of LECY 1 in boiling water (A), LECY 1 in 85/85 (B) and LECY 2 in 85/85(C).

composition versus time. Fig. 5 shows near-FTIR spectra for wet samples. Of particular note are the –OH peaks near 5000 cm^{-1} and 7000 cm^{-1}, the aromatic backbone peak near 6000 cm^{-1}, and the H_2O peak near 5250 cm^{-1}. Additionally, consistent with the mass uptake

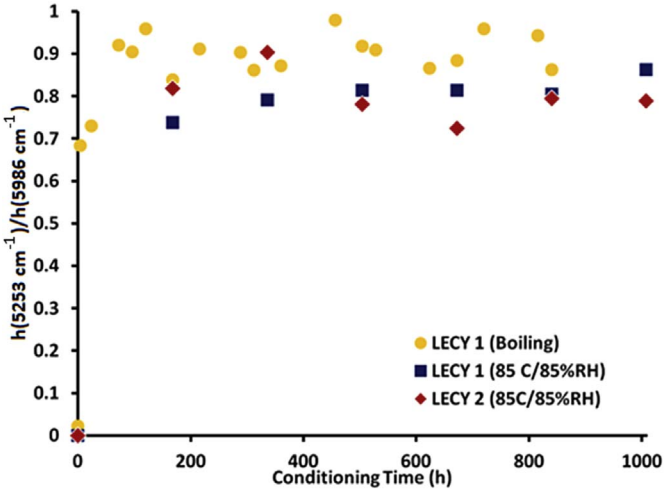

Fig. 6. FTIR traces for peak heights of 5253 cm^{-1}/5986 cm^{-1}.

results, the sample conditioned in boiling water showed more absorption at the H_2O peak (near 5250 cm^{-1}), indicating a higher water saturation level.

Fig. 6 shows the time-resolved traces of the H_2O relative peak heights for all three samples with respect to time. The peak goes up initially, but displays little change over the bulk of the experiment. These observations confirm that the initial mass increase corresponds to bulk water sorption and that water content is practically constant during the reaction. The water content at 85% relative humidity is very close to 85% of the saturation water content observed for water immersion, in line with previous observations of near-ideal Henry's law behavior for water in cyanate ester networks [37].

Fig. 7 shows the spectra of dry samples. While the 5250 cm^{-1} H_2O peak does not appear prominently (indicating that the samples are fully dried and do not retain residual moisture), the –OH peaks near 5000 cm^{-1} and 7000 cm^{-1} appear along with the aromatic backbone peak near 6000 cm^{-1}.

Fig. 8 shows the time-resolved FTIR peak values for the hydroxyl peak of dry samples, using the peak at 5000 cm^{-1} as the selected indicator of hydroxyl concentration. All samples show steady increases with respect to time, and provide an important measure of extent for the hydrolysis reaction.

3.3. Network degradation

Fig. 9 shows T_g plotted against exposure time for all samples. In all cases, the T_g decreases with time. The T_g drop is faster for LECY in boiling water than the other samples. LECY/GF samples have a higher initial T_g, but the relative T_g drop is similar to that of the other LECY samples with the same humidity conditioning.

4. Discussion

The mass uptake shown in Fig. 4 under humidification can be understood as bulk water sorption and network hydrolysis products. These two can be analytically distinguished and correlated with the FTIR peaks for H_2O and –OH, respectively. Once these values are determined on a molar basis, the data can be fit to pseudo-first order reaction kinetics. Finally, these kinetics can be used to understand the rate of network degradation and property loss. LECY/GF composites show anomalous behavior for both mass uptake and T_g.

4.1. Interpretation of mass uptake

Total mass uptake results given in Fig. 4 include weight gain effects

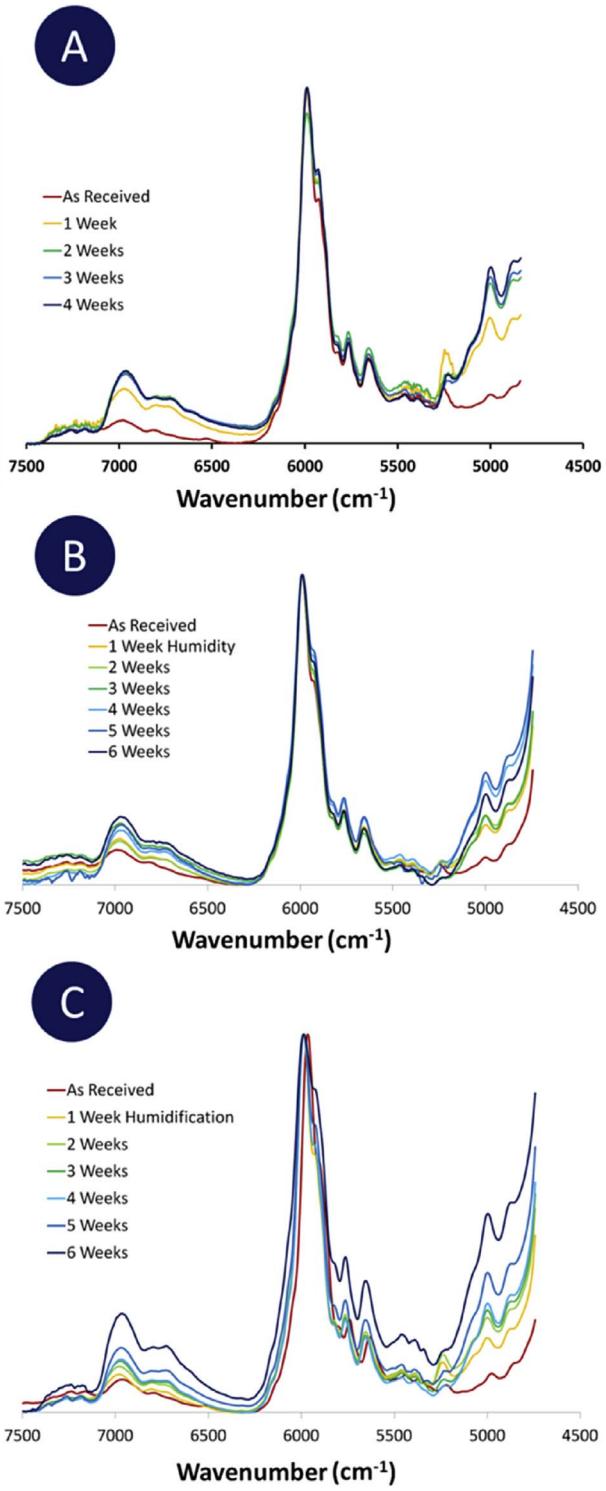

Fig. 7. FTIR traces for dry samples of LECY 1 in boiling water (A), LECY 1 in 85/85 (B), and LECY 2 in 85/85(C).

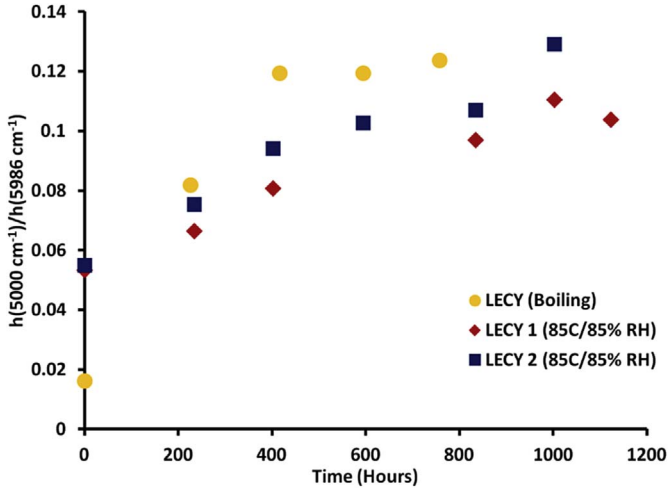

Fig. 8. FTIR traces for peak heights of 5000/5986 cm^{-1}.

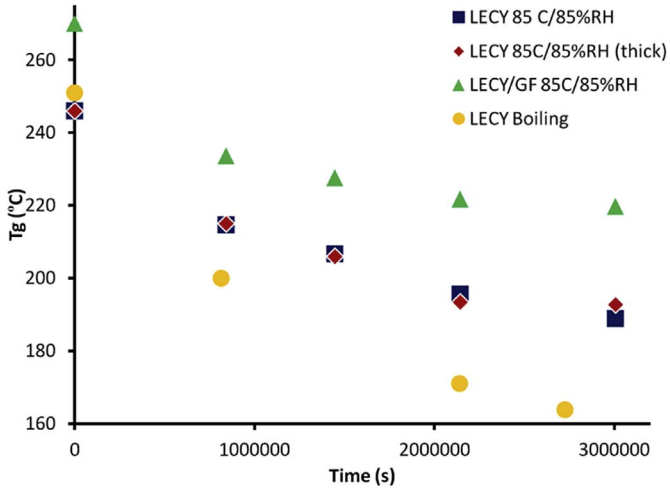

Fig. 9. T_g of exposed samples as determined by DMA vs. exposure time under all exposure conditions tested.

from both bulk sorption and cyanate ester hydrolysis products. Bulk sorption is reversible with humidity environment, while hydrolysis product formation is not. This is shown graphically in Fig. 10. In addition to the experimental data, reversible and irreversible mass uptake curves are calculated. Fig. 10a shows the irreversible dry uptake curve. This is a linear fit to weights of samples that have been conditioned and subsequently dried. Fig. 10b shows total mass uptake along with a calculated reversible mass uptake, corresponding to total water sorption. This is calculated by subtracting the irreversible mass uptake from the total mass uptake curve. This is taken to be bulk water diffusion, and confirms that, after initial diffusion, the concentration of water remains constant for the remainder of the experiment. The total uptake for LECY at near 100% conversion (due to the high-temperature post-cure) for these samples of 2.0–2.5% agrees well with previously reported values of 2.4% [38] and 2.3% [39] for 3 mm thick pucks with 96 h of immersion in water at 85 °C. Particularly at longer times, the irreversible mass changes in samples exposed to boiling water may be affected by extraction of small-molecule hydrolysis products. However, if such an effect were significant, the mass-IR calibration curve in Fig. 12 would show significantly different behavior for the samples exposed to boiling water as compared to those exposed only to humidity. Because such an effect was not clearly observed, and because quantification of this effect would be beyond the scope of the current work, we have retained the simplifying assumption of negligible extraction of small molecules during exposure to boiling water.

FTIR confirms the interpretation of the mass uptake results. Fig. 5 shows the linear increase of the hydroxyl stretching peaks (near 5000 cm^{-1} and 7000 cm^{-1}), corresponding to the irreversible mass uptake in Fig. 10a; Fig. 6 shows the FTIR traces for the wet samples, indicating that the total uptake is dominated by moisture uptake, as indicated by the reversible uptake curve in Fig. 10b.

These data are useful for calculating reaction kinetics. From the irreversible uptake data, the hydrolysis rate can be estimated directly via differentiation with respect to time. With the aid of a calibration

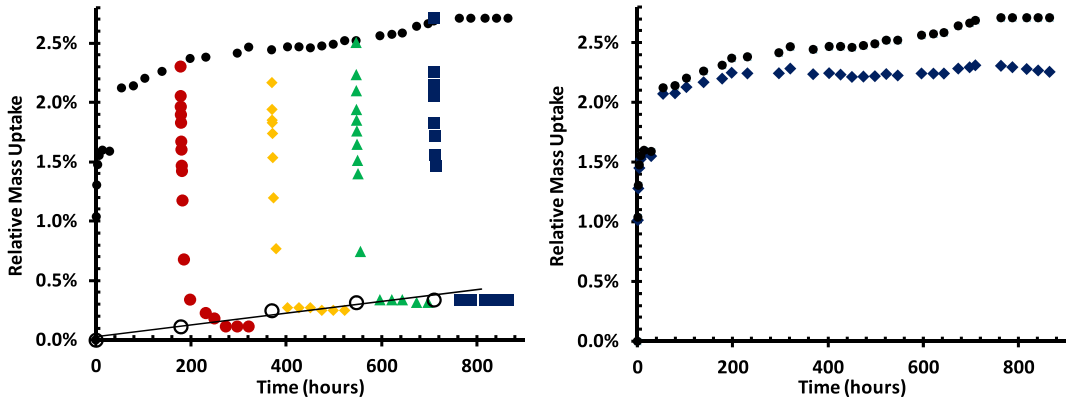

Fig. 10. Simple analysis performed on mass uptake curves for LECY 1 in boiling water. A) Raw uptake (●) and weekly drying curves(●,◆,▲,■) are shown, as in Fig. 7. Additionally, a linear fit to the drying curves is shown (○). This represents the mass uptake that is irreversible with respect to humidity environment and corresponds to the hydrolysis product formation. B) Total mass uptake (●) and environmentally reversible water uptake (◆). Environmentally reversible water uptake was calculated by subtracting the dry uptake from the total mass uptake.

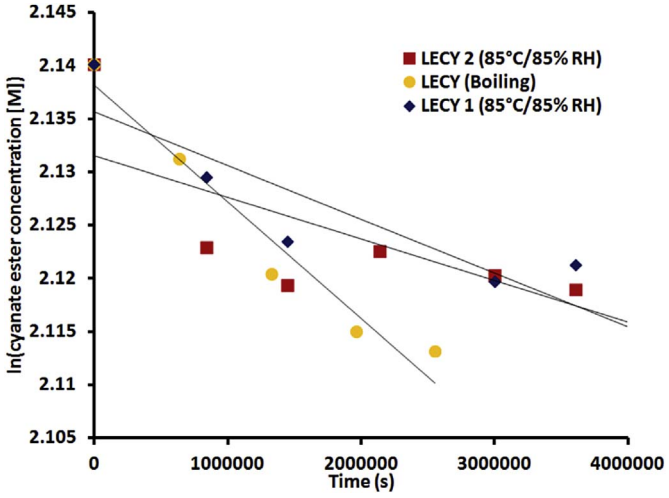

Fig. 11. Pseudo-first order kinetics fits from mass data only.

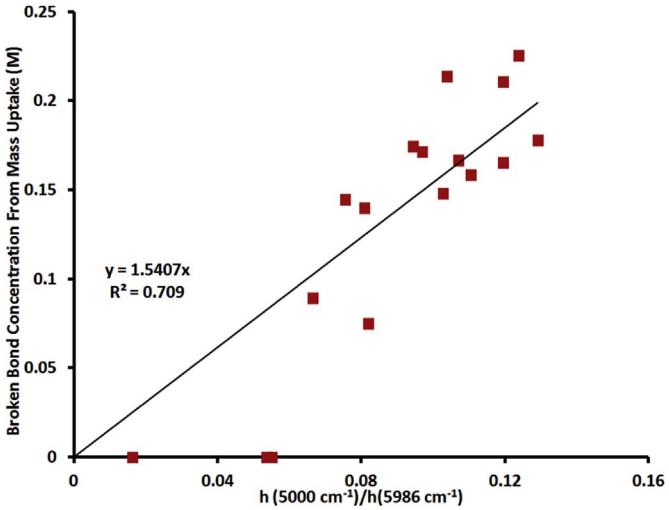

Fig. 12. Mass-IR calibration.

curve, a similar approach may be utilized with the FTIR data, either as a stand-alone method or for cross-validation of mass update data. In addition, the equilibrium water uptake curve is useful both to establish the water concentration during the experiment, both to test the validity of assumptions of constant concentration, and to determine the level of equilibrium water sorption for determination of true rate constants.

4.2. Determination of molar quantities

The conversion from fractional mass uptake to concentration can be determined, using:

$$C_{hE} = U \times \frac{1\ mole\ E_h}{mol\ H_2O} \times \frac{mol\ H_2O}{18\ g\ H_2O} \times \frac{1.2\ g\ LECY}{ml\ LECY} \times \frac{1000\ ml}{l}$$
$$= U \times \frac{66.67\ moles\ hydrolysis}{g\ H_2O/g\ LECY} \quad (2)$$

(where U is the mass uptake in mass percent, and C_{hE} is the concentration of hydrolyzed bonds). The total intact cyanurate bond concentration (C_E) can then be determined by:

$$C_E = C_{E0} - C_{hE} \quad (3)$$

where C_{E0} is the initial concentration of bonds subject to hydrolysis. For cured cyanate esters, there are three such bonds per cyanurate ring, and two per monomer, if the mechanism of Kasehagen [12] is assumed to account for all bond breaking caused by reaction with water. The number density of these bonds may be estimated based on the density of the cured network, along with the molecular weight, and functionality of the monomer:

$$C_{E0} = \frac{mole\ CE}{mol\ Monomer} \times \frac{1}{MW_{monomer}\left(\frac{g}{mol}\right)} \times \rho\left(\frac{g}{ml}\right) \times \frac{1000\ ml}{L} \quad (4)$$

For LECY with 2 mol CE/mole monomer, MW = 264 g/mol, and ρ = 1.2 g/ml at complete conversion of monomer to network [40], the maximum hydrolysable bond density is 9.08 mol/L.

In practice, however, full conversion is difficult to achieve, so 100% conversion cannot be assumed. Conversion can be estimated using experimental T_g and DiBenedetto parameters. Using literature values [41] for the DiBenedetto parameters, the samples in this study were estimated to have initial conversions ranging between 0.94 and 0.97, corresponding to an initial hydrolysable bond density of between 8.5 and 8.8 mol/L. These estimates are summarized in Table 1.

Table 1
Estimated conversion from T_g by literature DiBenedetto parameters.

	T_g (°C)	Conversion (by DiBenedetto parameters)	Hydrolysable Bond Density (mol/L)
LECY 1	251	0.943	8.5
LECY 2	246	0.943	8.5
LECY/GF	270	0.969	8.8

4.3. Reaction kinetics

4.3.1. Pseudo-first order reaction kinetics

Hydrolysis is hypothesized to occur following a simple rate law given by Equation (5) that is first order with respect to the concentrations of the two reactants – water and hydrolysable bonds. For the mechanism of Kasehagen [12], these bonds are aryl ethers denoted herein by –O–, with the understanding that only one of the denoted bonds is broken.

$$\frac{d[-O-]}{dt} = k\,[-O-][H_2O] \tag{5}$$

If the water concentration is assumed to be constant (an assumption that will be analyzed in the next section), this rate law can be simplified to a pseudo-first order rate equation with respect to the hydrolysable bond concentration:

$$\frac{d[-O-]}{dt} = k'\,[-O-] \tag{6}$$

(where k' = k[H_2O]). Eq. (6) can be solved by integration and yields the standard first order rate law:

$$[-O-] = [-O-]_0 e^{-kt} \tag{7}$$

Alternatively,

$$ln([-O-]) = -k't + ln([-O-]_0) \tag{8}$$

In this form, a plot of ln([-O-]) versus time would yield a slope of k' and an intercept of ln([-O-]$_0$).

4.3.2. Kinetic rate law fits

The simplest analysis of kinetic rate constants uses Equation (2) to establish concentrations from mass uptake data, and then uses those concentrations to fit for kinetics. Fig. 11 shows the resulting linear fit to Equation (8) for the unreinforced samples. Differences among the samples can be clearly seen. However, the quality of fit is generally poor. The poor fit may result from invalid assumptions about the reaction kinetics, or from errors in measurement of mass uptake. For all samples, the observed mass uptake was less than 0.2% of the polymer mass, corresponding to a mass uptake of less than 20 mg for these samples.

FTIR provides another method to qualitatively assess relative reaction extent. Additionally, the FTIR peak height data can be calibrated with mass uptake to provide concentration data with greater accuracy than mass uptake alone. Fig. 12 shows a calibration curve using data from all three experiments using a linear fit with a forced intercept of 0.

The resulting pseudo-first order kinetic fits are shown in Fig. 13. In order to arrive at the concentration values in Fig. 13, the IR peak heights were converted to broken bond concentrations using the calibration curve in Fig. 12. The y-axis values for the calibration curve were constructed by taking each measurement of irreversible mass gain after sample drying as equivalent to the quantity "U" in Equation (2), then computing a corresponding value of C_{he} (plotted as the y-axis in Fig. 12). In order to generate the y-axis values in Fig. 13, the measured FTIR absorbance of the hydroxyl peak near 5000 cm^{-1} was converted directly to a value for C_{he} using the calibration constant in Fig. 12, then the in-tact bond concentration C_E was computed with the aid of Equations (3) and (4). The natural log of C_E (divided by a reference concentration of 1 mol/L) was then used as the y-axis in Fig. 13. While the mass-IR fits retain the same general features as the fits generated by mass uptake data alone, the fits are much cleaner and the intercepts are closer to the expected original values. As expected, LECY samples conditioned in boiling water hydrolyzed significantly faster than the two 85 °C/85% RH samples. The two 85 °C/85% samples differed by about 20%. The pseudo first order kinetic parameters obtained from Figs. 11 and 13 are summarized in Table 2.

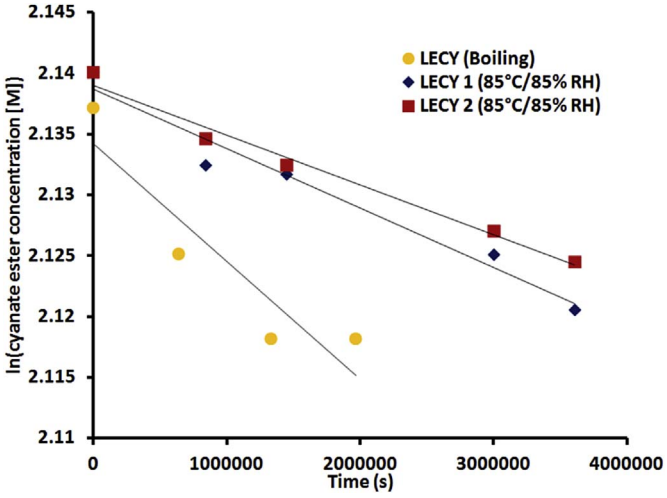

Fig. 13. Natural log of cyanate ester concentrations determined by mass-IR versus time, for linear fits to a pseudo-first order rate law.

Table 2
Pseudo first-order reaction rates by mass uptake and mass-IR.

	k'(s^{-1}) by mass uptake	R^2	k'(s^{-1}) by mass-IR	R^2
LECY (Boiling)	1.09×10^{-8}	0.95	9.7×10^{-9}	0.85
LECY 1(85 °C/85% RH)	5.05×10^{-9}	0.84	4.88×10^{-9}	0.96
LECY 2(85 °C/85% RH)	5.50×10^{-9}	0.56	4.08×10^{-9}	0.98
LECY/GF (85 °C/85% RH)	5.11×10^{-9}	0.44	n/a	

4.3.3. Assumption of constant water concentration and determination of true k values

Both FTIR (Fig. 6) and mass uptake data (see Figs. 4 and 10) indicate that the assumption of constant water concentration during the bulk of the experimental time window is a very good one. The technique illustrated in Fig. 10 provides a precise way to determine the equilibrium water concentration for the determination of the second order reaction rate values in combination with the pseudo-first order values previously estimated. The results are given I Table 3.

4.4. Relationship between T_g and extent of hydrolysis

The form of the T_g data in Fig. 9 appears similar across all samples, especially if the initial T_g of the system is taken into account. This similarity suggests the existence of an underlying fundamental relationship that can be utilized to determine, and perhaps even predict, the evolution of T_g in any given LECY system. Because of the well-defined nature of the cured cyanate ester network, there exists a fixed relationship between the T_g and the conversion, as described by the DiBenedetto equation introduced previously. In the absence of side reactions, there is an exact equivalence between "conversion" in terms of the disappearance of monomer, and what has been termed "network conversion" [42], or the extent of cross-link formation. In fact, the

Table 3
Pseudo reaction rates by mass-IR, equilibrium sorption, and true reaction rates.

	k' (s^{-1})	[H_2O]equil. (M)	k ($s^{-1}M^{-1}$)
LECY (Boiling)	9.70×10^{-9}	1.50	6.47×10^{-9}
LECY 1(85 °C/85% RH)	4.88×10^{-9}	1.41	3.46×10^{-9}
LECY 2(85 °C/85% RH)	4.08×10^{-9}	1.35	3.02×10^{-9}
LECY/GF (85 °C/85% RH)	5.11×10^{-9}	1.60	3.19×10^{-9}

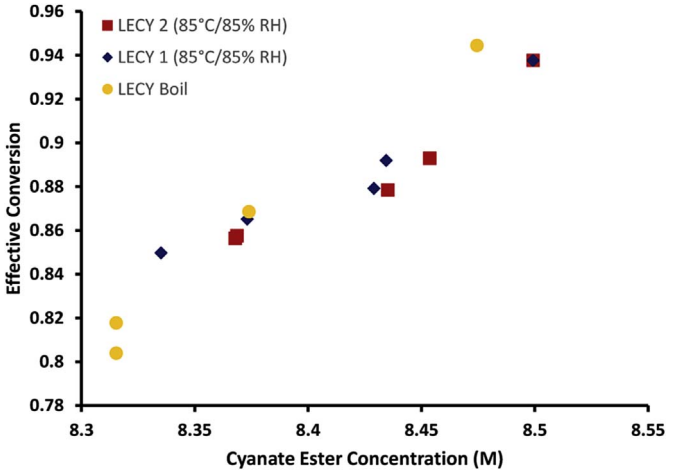

Fig. 14. Effective conversion as determined by T_g vs cross-link density as determined by mass-IR.

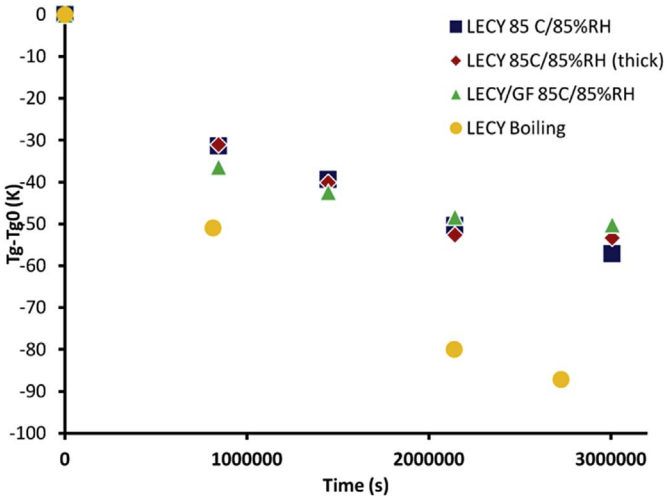

Fig. 15. Relative T_g dropoff for all samples across exposure time. Notably, although the composite samples had a higher initial T_g than the resin samples, there were no significant differences in T_g knockdown throughout the exposure.

"network conversion" in such a situation is directly proportional to the cross-link density of the system. Thus, the DiBenedetto equation may be described as a formal relationship linking cross-link density and T_g that is "universal" for a given network composition.

Although the DiBenedetto equation is nonlinear, there is still a one-to-one correspondence between "network conversion" and T_g, meaning that any given T_g may be translated into an "effective conversion" simply by inverting the DiBenedetto equation. Although in an ideal network with only monomers and a single type of cross-link, the "effective conversion" will be a linear function of cross-link density, even in a non-ideal network, we hypothesize that the "effective conversion" should be close to a linear function of cross-link density, and that this function should be the same for all hydrolyzed LECY networks. Using the mass-IR approach, an independent measure of cross-link density for the LECY networks under study is available (this measure was used to construct the y-axis of Fig. 13, for instance, and is independent of T_g). By converting the T_g of the hydrolyzed networks into "effective conversions" with the DiBenedetto parameters for LECY and plotting as a function of cross-link density, these hypotheses may be tested, as can be seen in Fig. 14. The figure shows a clear, nearly linear, and "universal" correlation between the remaining cross-link density as determined by mass-IR analysis and the independently-measured effective conversion as determined from T_g. In principle, this correlation should allow for the prediction of the evolution of T_g during hydrolysis for a sample once the kinetics of the hydrolysis reaction have been established.

4.5. LECY/GF composites

The LECY/glass fiber composites showed different behavior than the non-composite samples in several key ways. T_g was higher for both for unconditioned and conditioned samples (Fig. 9), although the T_g drop over time was similar. Additionally, the dry mass uptake over the course of the experiment was significantly higher than for pure LECY samples (Fig. 4), although the wet uptake data was consistent with that of neat polymer samples. For our experimental parameters, the glass fibers interfered enough with the near-FTIR source that analytical FTIR could not be accomplished.

The higher T_g of the post-cured glass fiber samples could be due to more thorough cure in the glass fiber samples, or due to network stiffening as a result of fiber presence. Despite the difference in initial T_g, however, T_g reduction (Fig. 15) shows glass fiber samples to behave similarly to neat polymer samples. Both the similar wet mass uptake rates and the correlation between T_g drop and humidification time suggests that the kinetics derived for neat polymer samples may be applicable to composite samples as well, when corrected for fiber fraction. A more thorough examination of the DiBenedetto equation parameters for glass-reinforced samples would enable "effective conversion" data to be computed. This data could then be used in conjunction with the universal relationship to cross-link density (Fig. 14) to arrive at an estimated extent of hydrolysis as a function of time. The estimated extent of hydrolysis in the reinforced networks could then be compared to the extent of hydrolysis observed in the equivalently conditioned neat resin networks to determine what effect, if any, reinforcement has on the kinetics of hydrolysis. This approach remains the subject of future work.

4.6. Comparison with PT-30 reaction rates

Previous work [34] used a similar approach to describe the degradation reactions of a triphenolic cyanate ester, Primaset PT-30. PT-30 has a higher cross-linking density, a significantly higher T_g, higher equilibrium water content, and a higher effective pseudo-first order hydrolysis reaction rate than LECY. Fig. 16 compares the density of hydrolysable bonds in LECY and PT-30 upon exposure to boiling water. Notably, although PT-30 exhibits an equilibrium water uptake which is significantly (2.5x) larger than that of LECY, this increase does not entirely account for the order of magnitude difference in pseudo first order hydrolysis rates. However, PT-30 contains a fairly complex

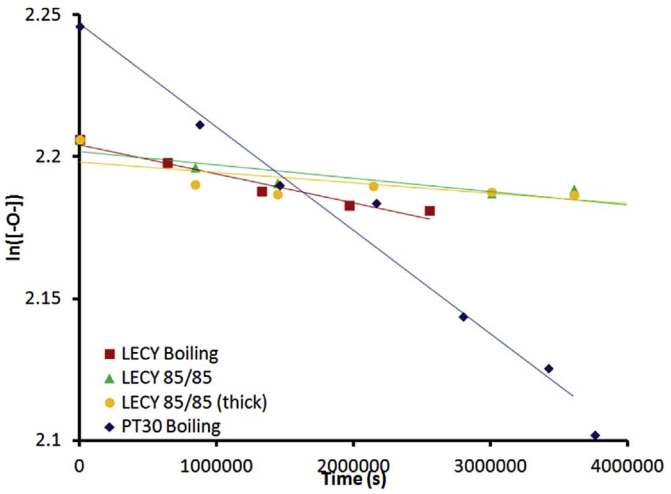

Fig. 16. Mass-derived concentrations for LECY and PT-30 samples versus time.

mixture of monomers and likely contains significantly different impurities than LECY, which could strongly impact hydrolysis rates. In particular, because the effects of differences in the chemical structure of the main ingredients in these cyanate ester networks cannot be separated from the influence of impurities, conclusions about the effects of differences in the chemical structure of the main ingredients are beyond the scope of this work.

5. Conclusions

Mass uptake and NIR spectroscopy were used to evaluate the degradation of a dicyanate ester thermoset. This technique measures the hydroxyl formation of intermediate phenol species, directly assessing the network-scission due to loss of hydrolysable bonds. From these results, we were able to determine a relationship between observed network degradation and changes in glass transition temperature.

Comparisons among samples exposed to boiling water and 85 °C/85% relative humidity showed that water uptake was slightly lower (in line with a linear sorption curve) for the samples conditioned at 85% humidity. Both pseudo-first order and true hydrolysis rates were significantly higher in the sample exposed to boiling water, as expected due to the higher exposure temperature. Although data on glass fiber-reinforced samples was more limited, the decline in T_g in these samples was found to evolve similarly to that of the near resin systems, albeit starting from a higher initial T_g. The rates of hydrolysis in LECY appeared to be significantly lower than those seen in earlier studies of PT-30 cyanate ester resin networks.

This work illustrates that the kinetics of hydrolysis in cyanate ester networks under a variety of conditions may be determined quantitatively using relatively straightforward procedures. With a small amount of initial data linking the extent of hydrolysis to glass transition temperatures under a limited set of conditions, it should be possible to develop predictions for the evolution of glass transition temperature during hydrolysis under a much wider set of conditions.

Competing interest statement

The authors declare no competing interest.

Acknowledgements

The support of the Air Force Research Laboratory and the Air Force Office of Scientific Research, project LRIR 16RQCOR361, is greatly appreciated.

References

[1] S. Das, D.C. Prevorsek, Cyananto Group Containing Phenolic Resins, Phenolic Triazines Derived Therefrom, United States Patent 4,831,086, (1989).
[2] S. Das, D.C. Prevorsek, B.T. Debona, 21st Int. SAMPE Tech. Conf, 1989, p. 972.
[3] I. Hamerton, Chemistry and Technology of Cyanate Ester Resins, Chapman & Hall, London, 1994, p. 357.
[4] X. Ning, J. Dang, X. Yue, J. Yuan, Properties analysis of novel composites for space robots, Polym. Compos. 35 (3) (2014) 564–569.
[5] P.D. Wienhold, D.F. Persons, The development of high-temperature composite solar array substrate panels for the MESSENGER spacecraft, SAMPE J. 39 (2003) 6–17.
[6] P.C. Chen, T.T. Saha, A.M. Smith, R. Romeo, Progress in very lightweight optics using graphite fiber composite materials, Opt. Eng. 37 (2) (1998) 666–676.
[7] D.A. Shimp, Technologically driven applications for cyanate ester resins, in: I. Hamerton (Ed.), Chemistry and Technology of Cyanate Ester Resins, Chapman & Hall, London, 1994, pp. 282–327.
[8] G. Wang, G. Fu, T. Gao, H. Kuang, R. Wang, F. Yang, W. Jiao, L. Hao, W. Liu, Preparation and characterization of novel film adhesives based on cyanate ester resin for bonding advanced radome, Int. J. Adhesion Adhes. 68 (2016) 80–86.
[9] A. Deutsch, C.W. Surovic, A.P. Lanzetta, H.A. Ainspan, J.C. Abbiate, A. Veihbeck, J.C. Hedrick, J.M. Shaw, S.L. Tisdale, E.F. Foster, P.W. Coteus, Broadband characterization of low dielectric constant and low dielectric loss CYTUF(TM) cyanate ester printed circuit board material, IEEE Trans. Compon. Packag. Manuf. Technol. Part B-Adv. Packag 19 (2) (1996) 331–337.
[10] V. Chidambaram, E.P.J. Rong, G.C. Lip, R.M.W. Daniel, Cyanate ester-based encapsulation material for high-temperature applications, J. Electron. Mater. 42 (9) (2013) 2803–2812.
[11] G. Wu, Y. Cheng, K. Wang, Y. Wang, A. Feng, Fabrication and characterization of OMMt/BMI/CE composites with low dielectric properties and high thermal stability for electronic packaging, J. Mater. Sci. Mater. Electron. 27 (6) (2016) 5592–5599.
[12] L.J. Kasehagen, I. Haury, C.W. Macosko, D.A. Shimp, Hydrolysis and blistering of cyanate ester networks, J. Appl. Polym. Sci. 64 (1) (1997) 107–113.
[13] A. Gitsas, T.D. Lazzara, B. Yameen, M. Steinhart, W. Knoll, H. Duran, Designing polymeric nanorod arrays for optical waveguide-based biosensors, Phys. Status Solidi C 8 (11–12) (2011) 3179–3182.
[14] H. Duran, B. Yameen, M. Geuss, M. Kappl, M. Steinhart, W. Knoll, Enhanced interfacial rigidity of 1D thermoset nanostructures by interface-induced liquid crystallinity, J. Mater. Chem. C 1 (46) (2013) 7758–7765.
[15] P. Abramian, F. de Aragon, J. Calero, J. de la Gama, L. Garcia-Tabares, J.L. Gutierrez, M. Karppinen, T. Martinez, E. Rodriguez, I. Rodriguez, L. Sanchez, F. Toral, C. Vazquez, Development of radiation resistant superconducting corrector magnets for LHC upgrade, IEEE Trans. Appl. Supercond. 23 (3) (2013) 4101204.
[16] A. Idesaki, T. Nakamoto, M. Yoshida, A. Shimada, M. Iio, K. Sasaki, M. Sugano, Y. Makida, T. Ogitsu, Development of high radiation-resistant glass fiber reinforced plastics with cyanate-based resin for superconducting magnet systems, Fusion Eng. Des. 112 (2016) 418–424.
[17] T. Hemmi, N. Koizumi, K. Matsui, K. Okuno, A. Nishimura, M. Sakai, S. Asano, Development of insulzition technology with Cyanate Ester resins for ITER TF coils, Fusion Eng. Des. 84 (2–6) (2009) 923–927.
[18] J. Hill, N. Munshi, M. Tupper, H. Babcock, A. Kintz, T. Kearns, A. Kimota, Risk mitigation for cyanate ester insulation of large magnets through cure optimization, IEEE Trans. Appl. Supercond. 25 (3) (2015) 1–5.
[19] J. Li, Z. Wu, C. Huang, L. Li, Gamma irradiation effects on cyanate ester/epoxy insulation materials for superconducting magnets, Fusion Eng. Des. 89 (12) (2014) 3112–3116.
[20] N.A. Munshi, J.K. Walsh, M.W. Hooker, H.K. Babcock, A.H. Haight, S.R. Durso, A. Kawaguchi, P. Hough, Radiation resistant electrical insulation qualified for ITER TF coils, IEEE Trans. Appl. Supercond. 23 (3) (2013) 7700104.
[21] K. Humer, R. Prokopec, H.W. Weber, H. Fillunger, R.K. Maix, Characterization and qualification of advanced insulators for fusion magnets, Fusion Eng. Des. 88 (5) (2013) 350–360.
[22] P. Fabian, M. Haynes, H. Babcock, M. Hooker, Characterization and qualification of cyanate ester/epoxy insulation for NSTX-U fusion magnets, IEEE Trans. Appl. Supercond. 23 (3) (2013) 7700204.
[23] F. Savary, R. Gallix, J. Knaster, N. Mitchell, K. Seo, The toroidal field coils for the ITER project, IEEE Trans. Appl. Supercond. 22 (3) (2012) 4200904.
[24] S. Pradhan, P. Brahmbhatt, J.D. Sudha, J. Unnikrishnan, Influence of manganese acetyl acetonate on the cure-kinetic parameters of cyanate ester-epoxy blend systems in fusion relevant magnets winding packs, J. Therm. Anal. Calorim. 105 (1) (2011) 301–311.
[25] M.W. Hooker, S.A. Arzberger, S.D. Grandlienard, M.W. Stewart, N.A. Munshi, G.M. Voss, R.D. Benson, M.S. Madhukar, Industrialization of radiation-resistant cyanate ester magnet insulation, IEEE Trans. Appl. Supercond. 19 (3) (2009) 2367–2370.
[26] A.W. Snow, The synthesis, manufacture, and characterization of cyanate ester monomers, in: I. Hamerton (Ed.), Chemistry and Technology of Cyanate Ester Resins, Blackie Academic, New York, 1994, pp. 7–57.
[27] V.V. Korshak, V.A. Pankratov, A.A. Ladovskaya, S.V. Vonogradova, Study of gel formation in the polycyclotrimerization reaction as typified by polycyanate synthesis, J. Polym. Sci. Polym. Chem. Ed. 16 (7) (1978) 1697–1707.
[28] C.P.R. Nair, D. Mathew, K.N. Ninan, Cyanate ester resins, recent developments, in: A. Abe, A.C. Albertsson, H.J. Cantow, K. Dusek, S. Edwards, H. Hocker, J.F. Joanny, H.H. Kausch, T. Kobayashi, K.S. Lee, J.E. McGrath, L. Monnerie, S.I. Stupp, U.W. Suter, G. Wegner, R.J. Young (Eds.), New Polymerization Techniques and Synthetic Methodologies, Springer, Berlin, 2001, pp. 1–99.
[29] A. Osei-Owusu, G.C. Martin, J.T. Gotro, Analysis of the curing behavior of cyanate ester resin systems, Polym. Eng. Sci. 31 (22) (1991) 1604–1609.
[30] R.H. Yeh, P.W. Lin, K.F. Lin, Two-stage moisture absorption behavior and hydrolysis of cured dicyanate ester resins, J. Polym. Res.-Taiwan 9 (1) (2002) 31–36.
[31] D.A. Shimp, S.J. Ising, Moisture effects and their control in the curing of polycyanate resins, PMSE Preprints (1992) 504–504.
[32] T.B. Colwell, C. Jacob, M. Messana, Assessing the Sensitivity of Cyanate Ester Composites to Carbamate Damage, Society for the Advancement of Material and Process Engineering, 2011, pp. Colwell/1–Colwell/15.
[33] R.J. Zaldivar, J.P. Nokes, Identification and evaluation of progressive thermal degradation caused by carbamate formation in cyanate ester resin-based composites, Polym. Eng. Sci. 51 (1) (2011) 158–169.
[34] V.V. Marella, J.A. Throckmorton, G.R. Palmese, Hydrolytic degradation of highly crosslinked polyaromatic cyanate ester resins, Polym. Degrad. Stabil. 104 (2014) 104–111.
[35] M. Gaku, Properties and applications of bisphenol A type cyanate resin, Polym. Mater. Sci. Eng. 71 (1994) 621–622.
[36] V.V. Korshak, P.N. Gribkova, A.V. Dmitrenko, A.G. Puchin, V.A. Pankratov, S.V. Vinogradova, Thermal and oxidative thermal degradation of polycyanates, Polym. Sci. USSR 16 (1) (1974) 15–23.
[37] S.K. Karad, F.R. Jones, Mechanisms of moisture absorption by cyanate ester modified epoxy resin matrices: the clustering of water molecules, Polymer 46 (8) (2005) 2732–2738.
[38] A.J. Guenthner, K.R. Lamison, V. Vij, J.T. Reams, G.R. Yandek, J.M. Mabry, New insights into structure-property relationships in thermosetting polymers from studies of cocured polycyanurate networks, Macromolecules 45 (1) (2012) 211–220.
[39] A.J. Guenthner, M.W. Wright, A.P. Chafin, J.T. Reams, K.R. Lamison, M.D. Ford,

S.P.J. Kirby, J.J. Zavala, J.M. Mabry, Mechanisms of decreased moisture uptake in ortho-methylated di(cyanate ester) networks, Macromolecules 47 (22) (2014) 7691–7700.
[40] J.T. Reams, A.J. Guenthner, K.R. Lamison, V. Vij, L.M. Lubin, J.M. Mabry, Effect of chemical structure and network formation on physical properties of di(cyanate ester) thermosets, ACS Appl. Mater. Interfaces 4 (2) (2012) 527–535.
[41] A.J. Guenthner, J.T. Reams, K.R. Lamison, S.M. Ramirez, D.D. Swanson, G.R. Yandek, C.M. Sahagun, M.C. Davis, J.M. Mabry, Synergistic physical properties of cocured networks formed from di- and tricyanate esters, ACS Appl. Mater. Interfaces 5 (17) (2013) 8772–8783.
[42] A.J. Guenthner, C.M. Sahagun, K.R. Lamison, J.T. Reams, T.S. Haddad, J.M. Mabry, Effect of nanoparticle functionalization on the performance of polycyanurate/silica nanocomposites, Ind. Eng. Chem. Res. 55 (26) (2016) 7096–7107.